Journal of Intelligent Systems and Internet of Things
Vol. 17, No. 02, PP. 295-310-, 2025
DOI: https://doi.org/10.54216/JISIoT.170219

Low-Cost Multi-Sensor Localization for Indoor AGVs

Nopparut Khaewnak [1], Siripong Pawako[1], Akkharachai Kosiyanurak[1], Suradet Tantrairatn[1], Jiraphon Srisertpol[1,*]

[1]School of Mechanical Engineering, Institute of Engineering, Suranaree University of Technology), Nakhon Ratchasima, Thailand

Emails: d6500412@g.sut.ac.th; siripongpawako@gmail.com; m6501891@g.sut.ac.th; suradetj@sut.ac.th; jiraphon@sut.ac.th

Abstract

Indoor transportation systems are a key area of development, where Automated Guided Vehicles (AGVs) help to increase efficiency and reduce labor costs. However, high-precision positioning technologies such as LiDAR and GNSS are expensive, making them unsuitable for widespread use. This research has developed a low-cost positioning system for indoor AGVs using multiple sensors, including CCTV, UWB, inertial measurement units (IMUs), and encoders. The experiment was carried out under both static and dynamic conditions. In static tests, Trilateration distance measurements show a lower positioning error than the triangular method, with a maximum error of 1.4464 m (x-axis) and 1.0464 m (y-axis) in dynamic tests. The integrated Encoder and IMU sensor data yielded the lowest error (RMSE = 0.0732 m at 0.4 m/s, 0.0678 at 0.27 m/s), Next is CCTV, while UWB has the highest error rate. The application of a Parallel Sensor Fusion architecture optimized using a Generalized Reduced Gradient (GRG) nonlinear algorithm, significantly reduced localization errors. The RMSE values decreased to 0.0623 m (0.4 m/s) and 0.0411 m (0.27 m/s). The results, in a controlled environment laboratory, indicate that combining multiple sensors will improve the positioning accuracy. Combining the encoder and IMU effectively reduces accumulated errors and increases system stability. While Adjust the weight of the sensor offline, this proposed system offers a cost-effective positioning solution for indoor AGVs, which contributes to the development of affordable and accurate AGV navigation systems.

Received: January 01, 2025 Revised: March 01, 2025 Accepted: June 05, 2025

Keywords: Automatic Guided Vehicles (AGVs); Positioning Technology; Low-cost Sensors; Multi-Sensor Fusion; Localization

1. Introduction

Freight transportation is fundamental to the manufacturing industry. Starting with human and animal labor, assistive devices such as trolleys and conveyors have been developed to increase transportation efficiency [1]. Modern smart factory transportation systems, a key component of Industry 4.0, are designed to operate automatically. Automated Guided Vehicles (AGVs) are intelligent systems that increase accuracy and reduce costs. These AGVs act as “delivery vehicles”, communicating within the Internet of Things (IoT) system by collecting and transmitting data through a centralized control system. However, AGVs used in industrial factories operate indoors.

AGVs used in industrial facilities often operate in indoor environments where satellite positioning systems such as the Global Positioning System (GPS) or Global Navigation Satellite System (GNSS) are not accurately operational because the signal is interfered with by obstacles [2, 3]. This challenge has driven advances in indoor positioning technologies, including the Affordable Indoor Navigation Solution (AINS) [4], which has different types of sensors for positioning. Automated guided vehicles (AGVs) rely on various sensors for precise positioning and navigation. Among these, LiDAR (Light Detection and Ranging) is the most widely used technology due to its high accuracy and accuracy in environmental mapping [5]. The high cost is still a major disadvantage [6, 7]. Cameras are also often used to create maps and detect objects. However, conventional monoculer cameras cannot

measure depth [8, 9], so accessories such as ArUco markers [10] or light-emitting diode panels [11] are required. (LED) for better spatial perception.

Inertial units (IMUs) are used to track the movement of AGVs, but their accuracy decreases over time due to accumulated errors [12]. While these technologies can improve AGV navigation efficiency, the high cost of LiDAR and camera limitations have prompted research into cost-effective alternative positioning solutions [13]. New approaches such as Ultra-Wideband (UWB), closed-circuit television (CCTV), IMUs, and encoders are being considered to replace LiDAR sensors in the indoor AGV, Which provides a reasonable price for accuracy

Ultra-wideband (UWB) technology is a reliable solution for AGV positioning, however, the performance of this technology depends on optimal transmitter positioning to ensure accurate line-of-sight (LoS) transmission [14]. The accuracy of this technology can be further improved by incorporating Kalman filters to reduce noise and improve state estimation [15]. In addition, closed-circuit television (CCTV), a technology that is widely used in industrial environments, is widely used in industrial environments. AGV navigation can be supplemented by route monitoring and identifying areas with a high density of obstacles, which improves overall performance [16].

Sensor integration is an important technique to reduce errors and increase the accuracy of low-cost sensors in AGV navigation. The sensor data is processed sequentially, and the processing is parallel, where multiple sensors operate simultaneously. A hybrid approach that combines the two methods can further optimize the sensor by taking advantage of the strengths of each [17–19].

The integration of multiple sensors greatly improves the positioning accuracy of AGVs. For example, combining UWB and LiDAR yields an average squared error (RMSE) of 36.3 cm, while combining Odometry and LiDAR yields an RMSE of 43.4 cm [20].

While numerous techniques have been developed for indoor AGV localization through sensor fusion, many existing studies still rely on expensive sensors like LiDAR or RGB-D cameras, making them unsuitable for cost-sensitive AGV platforms. Additionally, there has been relatively little attention paid to how real-world factors—such as sensor noise and inconsistent sampling rates—impact localization accuracy when using affordable, mixed-sensor setups like UWB, CCTV, IMU, and encoders. Therefore, the objective of this research is to develop a low-cost, multi-sensor localization framework for indoor AGVs. The proposed system integrates UWB, CCTV, IMU, and encoder data using a parallel sensor fusion structure. A Generalized Reduced Gradient (GRG) optimization algorithm is employed to dynamically determine the optimal sensor fusion weights that minimize positioning Root Mean Square Error (RMSE) in varying speeds. This document is structured as follows: Part II describes in detail the positioning methods and functions of each sensor used in this study. Part III describes the characteristics of the sensor. Part IV presents the results of the experiment. Analyse positioning accuracy for fixed conditions and move at different speeds. In addition, Generalized Reduced Gradient (GRG) techniques are used to optimize calculations in determining the optimal sensor set. Although Kalman Filter is popular, this research uses GRG to reduce the computational resources for optimum sensor weighting configuration. Part V summarizes the findings and key conclusions of this research.

2. Material and Methods

In this section, we describe the methodology for determining the position and function of each type of sensor used in this research. The study employs the BALTY AGV, an autonomous mobile robot equipped with multiple sensors, designed to determine its position within the experimental area, as illustrated in Figure 2. To minimize costs, the system utilizes low-cost sensors instead of LiDAR, which is commonly used in traditional positioning but is expensive.

The developed positioning system integrates internal and external sensor data to achieve high accuracy. The AGV positioning process can be divided into two main approaches: (1) internal positioning, which is inside the AGV such as encoders and IMUs, and (2) external positioning, which uses external sensors such as UWB and CCTV. By combining data from multiple sensors.

2.1 System Architecture and IoT Integration

The presented AGV operational concept is semi-autonomous. The core of the processing is the Jetson Nano board connected to the teensy board to control the JGB37-520 DC motor for navigation and obstacle avoidance. The system uses a Camera (Tapo C200) as the main sensor for image processing to allow the robot to move along the specified path, along with Ultrasonic Sensors installed to detect and avoid obstacles, as shown in Figure 1.

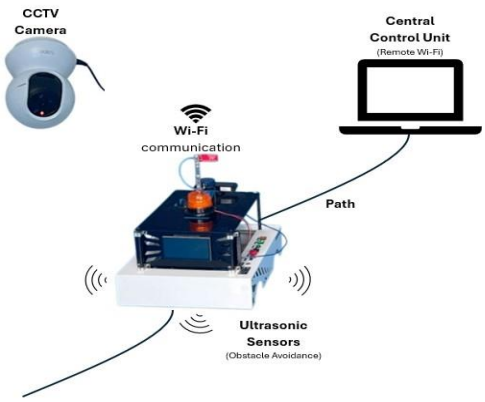

Figure 1. Conceptual Diagram of AGV Operation with CCTV, Ultrasonic Sensors, and Central Wi-Fi Control.

The BALTY AGV robot (as shown in Figure 2) is used for localization. The system integrates both Internal and external sensors. Internal sensors include a motor encoder for estimating position from PWM signals and an IMU (WitMotion WT901C) for measuring movement direction. External sensors include a UWB module (ESP32 UWB DW1000) used to measure the distance between tags mounted on the AGV and anchors placed around the test area. Additionally, a CCTV camera (Tapo C200) is used to process images to determine the AGV's location. Data from all sensors is transmitted over a Wi-Fi network using the MQTT protocol for real-time communication. The data is then forwarded to the Central Control Unit (CCU) (as shown in Figure 3), which is crucial for data fusion, route planning, and traffic management. Moving the processing load to the CCU significantly reduces hardware costs and complexity on each robot, while increasing accuracy and coordination capabilities across multiple AGVs.

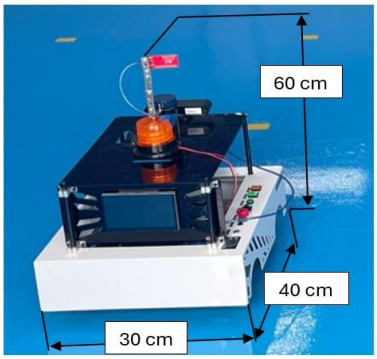

Figure 2. AGV BALTY ROBOT.

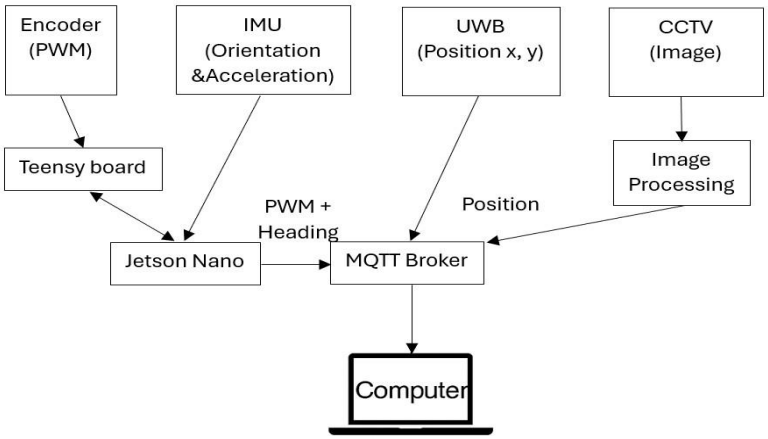

Figure 3. Communications of sensors.

2.2 Sensor Specifications

2.2.1 Encoder Sensor

The encoder is a sensor attached to the DC Motor (JGB37-520) located on the back of the motor shaft. This encoder uses a Double Magnetic Hall Encoder Disc that provides an AB-phase (Quadrature Signal) output signal. This makes it possible to analyze the direction and number of revolutions of rotation. An operating voltage of 3.3–5 V DC provides a frequency signal of 90 pulses per revolution of the motor shaft, as shown in Figure 4.

Figure 4. DC Motor with Encoder Sensor.

2.2.2 Inertial Measurement Unit Sensor

IMU (Inertial Measurement Unit) WitMotion WT901C is a 9-axis sensor (9 DOF – Degrees of Freedom) that can measure a variety of values, including linear acceleration, rotational rate, and other factors. The WT901C supports measurement of acceleration in the range of ±16g and rotational rates of up to ±2000 degrees per second (°/s). In this study, the output rate of the IMU is configured to 10 Hz, as shown in Figure 5.

Figure 5. IMU Sensor.

2.2.3 UWB Sensor

UWB consists of an ESP32 UWB board equipped with a DW1000 module, which can transmit and receive UWB wave signals for distance measurement with Time of Flight (ToF) techniques and distance estimation based on signal strength or RSSI (Received Signal Strength Indicator), as shown in Figure 6. The Anchor installation is defined at the 4 points of a 4×8 meter rectangular area, fixed to the bracket perpendicular to the ground, so that the signal can be received evenly from all directions, as shown in Figure 8. The tag mounted on the AGV measures the distance from the anchor at 4 points to calculate the 2D coordinates by trilateration or triangulation technique, and then sends the location coordinates back to the central processor via WiFi using the MQTT protocol.

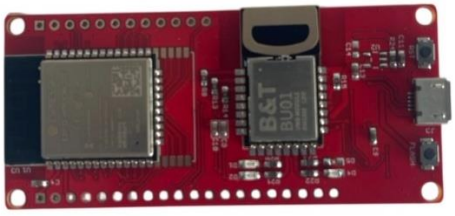

Figure 6. UWB Sensor.

2.2.4 CCTV

There are 4 CCTVs used in the system, that is TP-Link Tapo C200, which is a wireless IP camera (WiFi Camera) that can be connected via a wireless network to transmit images directly to the central processing system. The CCTV also supports low-light operation with infrared at a wavelength of 850 nm (850 nm IR LED), which can be seen at a distance of up to 30 feet. This camera comes with a lens with an f/NO aperture of 2.4 and a focal length of 4 mm. This is ideal for indoor medium-distance photography. The camera can record video at the highest resolution of Full HD (1080p) at 30 frames per second. It uses the H.264 video compression standard to efficiently transmit real-time image data over a WiFi network, as shown in Figure 7.The CCTV is installed at four CCTV cameras of the indoor experimental area (4 m × 8 m), as shown in Figure 8.

Figure 7. CCTV Sensor.

2.3 Localization Techniques

AGV localization has both outdoor localization that can use GPS sensors, CCTV, and Lidar, which is the main sensor for localization, and indoor localization cannot use GPS sensors. Most of the users will use LiDAR CCTV for localization but the price of LiDAR is high so it is the origin of using low-cost sensors, which will be localized in 2 forms according to the reading of the sensor.

2.3.1 Internal Localization (Encoder and IMU)

Localization determination from inside the AGV is done by using sensors to measure values from the AGV itself. The internal sensors measure values from the encoder and the IMU. AGV localization determination from the encoder sensor and its integration with heading Localization determination of an AGV using a two-wheel differential drive system can be efficiently achieved by combining information from the initial encoders with a mathematical model of the AGV, as shown in Figure 9(a).

The position of the AGV can be found by defining two coordinate systems. The first coordinate system is the global coordinate system on the frame (X_0, Y_0) and the second system is the robot coordinate system (X_r, Y_r) as shown in Figure 9(a). It can be seen that the two frames are defined, with the origin of the robot frame set to be the midpoint A on the axis between the wheels, the center of mass C of the robot is considered to be on the axis of symmetry, at a distance d from the origin A, with the radius of the wheel R and the distance from the center of the wheel L.

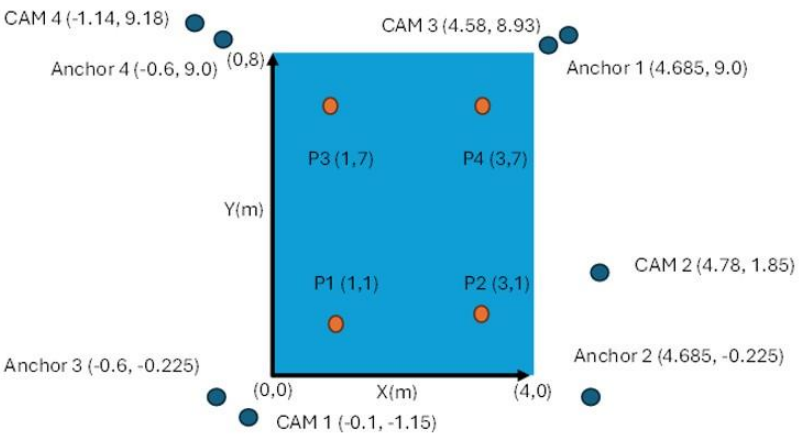

Figure 8. CCTV Sensor.

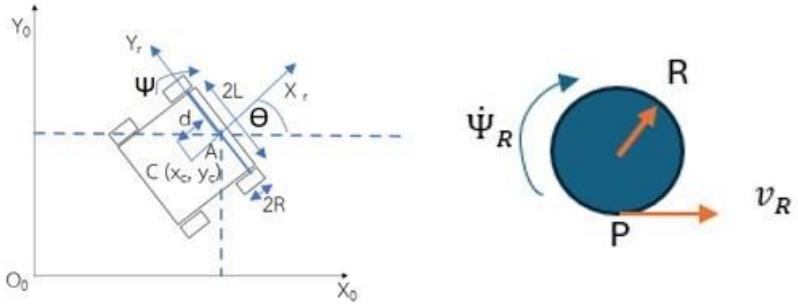

(a) Differential drive [21] (b) Right wheel [22]

Figure 9. Two components of the robot.

The kinematics and dynamics modelling of a two-wheeled self-driving AGV (DDMR, Differential Drive Mobile Robots) is designed since this equation describes the relationship between the velocity and the robot frame. The motion of the DDMR is characterized by non-holonomic constraint equations based on a set of assumptions [22, 23]. The first assumption is that there is no sliding motion. This constraint only means that the robot can move in a curved manner (forward and backward), but not sideways. In the robot frame, this assumption means that the velocity of center A is zero. The second assumption is the rotation of the wheels. There is one point of contact P with the ground as shown in Figure 9(b). There is no wheel slip in the longitudinal axis (X_r) and no slip in the perpendicular axis (Y_r). The velocity of the contact point in the robot frame is related to the velocity of the driven wheels in conjunction with the robot geometry, where the linear velocity of each driven wheel is the average of the linear velocities of the two wheels.

$$v = \frac{v_R + v_L}{2} = R\frac{\dot{\varphi}_R + \dot{\varphi}_L}{2} \quad (1)$$

Where v_R is the speed of the right wheel (m/s), v_L is the speed of the left wheel (m/s), $\dot{\varphi}_R$ is the angular speed of the right wheel (rad/s), $\dot{\varphi}_L$ is the angular speed of the left wheel (rad/s), And the angular velocity of DDMR, i.e.,

$$\omega = \frac{v_R + v_L}{2L} = R\frac{\dot{\varphi}_R - \dot{\varphi}_L}{2L} \quad (2)$$

To determine the position and velocity, it can be calculated as a function of velocity from the center of A, i.e.,

$$\begin{aligned} X &= X_A + vdt\cos\theta \\ Y &= Y_A + vdt\sin\theta \\ \dot{X} &= \dot{X}_A + v\cos\theta \\ \dot{Y} &= \dot{Y}_A + v\sin\theta \\ \theta &= \theta_0 + \omega dt \end{aligned} \quad (3)$$

Where X is the position in the x-axis, Y is the position in the y-axis, $\dot{X}$ is the velocity in the x-axis of the AGV, $\dot{Y}$ is the velocity in the y-axis of the AGV, $\dot{X}_A$ is the velocity in the x-axis of point A, $\dot{Y}_A$ is the velocity in the y-axis of point A, θ_0 is the initial angle of the AGV concerning the x-axis, dt is the change in time (Delta-time), θ is the angle of the AGV or heading of the AGV. and read the heading from the IMU sensor as an angle and use to replace the angle that occurs.

2.3.2 External Localization (UWB and CCTV)

External positioning is the use of external sensors to measure the position of an object, which is often already in use and is a low-cost sensor. Positioning from the sensor has

2.3.2.1 Localization from UWB sensor

UWB (Ultra-Wideband) position tracking from the Received Signal Strength Indicator (RSSI) and distance (d) obtained from 3 UWB sensors [24]. The distance d can be calculated from the RSSI using the equation.

$$d = 10^{\frac{A - RSSI}{10n}} \quad (4)$$

Where A is the measured signal strength at a 1-meter distance (dBm), RSSI is the measured signal strength (dBm), and n is the path loss exponent.

Another method is to use the distance from the UWB Time of Flight (ToF) to calculate the location by measuring the distance based on the time the signal travels from the Tag to the Anchors, which uses Ultra-Wideband (UWB).

From both methods, distance can be measured, which is divided into 2 calculation methods. When the distances d_1, d_2, and d_3 from the 3 UWB sensors (Anchor 1, Anchor 2, Anchor 3) from the positions (X_1, Y_1), (X_2, Y_2) and (X_3, Y_3) of the UWB sensors, respectively, the trilateration principle can be used to calculate the position (X, Y).

$$(X - X_1)^2 + (Y - Y_1)^2 = d_1^2 \quad (5)$$

$$(X - X_2)^2 + (Y - Y_2)^2 = d_2^2 \quad (6)$$

$$(X - X_3)^2 + (Y - Y_3)^2 = d_3^2 \quad (7)$$

From Eq. (5, 6 and 7) we can solve this system of equations to find the x and y positions of the AGV.

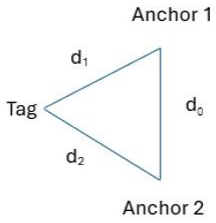

Figure 10. The triangular method.

Method 2 uses the trigonometry principle, using trigonometry equations, to find the distances d1 and d2 from the two UWB sensors (Anchor 1 and Anchor 2) from the positions (X_1, Y_1) and ((X_2, Y_2) of the UWB sensors, respectively, and the distance between Anchor 1 and Anchor 2 (d_0) is shown in Figure 10. using the equation.

2.3.2.2 Localization from CCTV

For localization tracking use CCTV to find coordinates. From the image in the area of interest and the location, it can be seen that the image is distorted due to the lens inside the camera, which is corrected by placing the image on a chessboard and detecting it. The image is passed through a mathematical model with a regression coefficient to create a straight line and the robot's position can be determined using an algorithm to detect and locate objects from images [25].

2.4 Multi-Sensor Data Fusion Algorithm

2.4.1 Parallel Fusion Algorithm

Fusion sensor architectures are divided into three types: series: operation based on one output as the next, parallel: Simultaneous operation and combination: series and parallel fusion, with the architecture divided into two types according to the type of data fusion: the first type is voting, weighting, and priority voting, and the second type is divide and conquer. The dataset is divided into subsets of the same size. The classification is then carried out, followed by the inclusion of decision data based on the results of those subsets of the classification [18].

2.4.2 Generalized Reduced Gradient (GRG) Method: A Nonlinear Optimization Algorithm

The Generalized Reduced Gradient (GRG) method is an effective algorithm used to solve non-linear optimization problems, extending the capabilities of the Reduced Gradient method by effectively addressing the constraints of inequality. The process starts by dividing the variable into a base variable (y) and a non-base variable (x) and then reducing the dimension of the problem by displaying y as a function of x, resulting in the target function $F(x) = f(y(x), x)$. This method turns the problem into a minimized $F(x)$ within the scope of $l \leq x \leq u$ [26, 27].

$$\Delta F(x) = \frac{\partial f}{\partial x} - \frac{\partial f}{\partial y}\left(\frac{\partial g}{\partial y}\right)^{-1}\frac{\partial g}{\partial x} \quad (8)$$

where:

$\frac{\partial f}{\partial x}, \frac{\partial f}{\partial y}$ *are the gradients of the objective function.*

$\frac{\partial g}{\partial x}, \frac{\partial g}{\partial y}$ *are the Jacobian matrices of the constraints.*

GRG is a precise and versatile algorithm for the computation of nonlinear equations. This algorithm is commonly used in software such as Microsoft Excel Solver [28, 29], leveraging techniques such as numerical differentiation and lower-upper factorization to optimize [26, 27] calculations. The GRG stands out for its complex equation management, making it ideal for using [30]. This algorithm requires heavy computation, especially for large matrices, and that converges into a locally appropriate value instead of a generic optimal value [29]. Starting the parameters correctly is considered important for achieving optimal results. Despite these challenges, GRGs remain a powerful tool for non-linear computations due to their robustness and flexibility in reducing selected error statistics [30].

In this study, the GRG algorithm was applied offline to find the most appropriate weighting coefficients (a, b, c, d, and e) for the sensor fusion model. This process is not a real-time adjustment, but rather, the pre-recorded data from each path were processed using the Solver tool in Microsoft Excel. The GRG Nonlinear method was used to adjust the weighting coefficients until the lowest Root Mean Square Error (RMSE) was obtained when comparing the path obtained from the fusion to the ground truth path. This pre-calculated optimal weighting coefficient set was then used in the sensor fusion model for the experiment.

3. Experimental Design

The experimental design in this study focuses on the use of low-cost sensors to localize AGVs and partition the experiments into two main parts: static experiments and dynamic experiments to verify the accuracy of the sensors and the performance of the data fusion techniques. For the static experiment, the test is performed in a predetermined localization within a 4x8 square meter test area, testing position readings from external sensors such as UWB and CCTV, and comparing the different techniques used to calculate the position. The dynamic experiment focuses on the localization test while The AGV moves in a straight line under specified conditions, collecting position data from UWB and CCTV, as well as Pulse Width Modulation (PWM) from encoders and direction values from IMUs, which can be used to analyse and improve the accuracy of the AGV's positioning system. Both of these experiments aim to evaluate the capabilities of various sensors and improve the accuracy of AGV positioning so that they can be used as a practical guideline.

3.1 In static experiments

In experiments, four conditions are determined: (1,1), (3,1), (1,7), and (3,7), as shown in Figure 8, within a 4x8 square meter test area. The AGV moves in four directions at angles of 0, 90, 180, and 270 degrees relative to the x-axis, repeating each movement three times. The installation points of UWB and CCTV anchors are shown in Figure8. The study involves comparing Time-of-Flight signal readings with RSSI reading methods, evaluating the use of the 3P method (trilateration) against the 2P method (triangular), analyzing the position of anchors used in calculations, and comparing UWB and CCTV for localization accuracy.

3.2 In dynamic experiments

In experiments, linear motion is analysed by collecting position data from UWB in the specified conditions, obtaining location data from CCTV, which are processed using a vision-based localization algorithm [25], gathering Pulse Width Modulation (PWM) data from encoders, and recording vehicle direction data from the IMU at average speeds of 0.27 m/s and 0.4 m/s. The study involves comparing movement data obtained solely from the encoder with data incorporating direction readings from the IMU, utilizing average Weighted Parallel Fusion, applying Weighted Parallel Fusion customized in Microsoft Excel for each moving path, and implementing Weighted Parallel Fusion from combined path customizations in Microsoft Excel.

3.3 Timestamp and Communication Management

To ensure data integrity for the data fusion algorithm, the data collection process has specific sampling rates: 10 Hz for UWB IMU wheel encoders and 5 Hz for CCTV. Since data from each sensor is collected asynchronously, the temporal alignment is performed using event-based synchronization in the post-processing step. We set the 'AGV start of movement' as the reference marker to synchronize all datasets. For sensor data communication, the MQTT protocol is used, which has a basic QoS configuration that emphasizes fast data transmission. However, this method may occasionally cause data loss under unstable Wi-Fi network conditions.

4. Results and Discussion

This experiment was divided into two types, namely a Static Experiment, and a Dynamic Experiment, to study the accuracy of the location of each sensor, which consisted of UWB, CCTV, IMU, and Encoder. After that, the position values obtained from each sensor were used to fuse the data (Parallel Fusion) to find the best results. For UWB positioning, the ESP32 DW1000 UWB Module BU01 is used, with anchors placed at all four corners, as shown in Figure 5. The tag is mounted at the center of the AGV. The system reads the signal data as the distance

between the anchors and the tag, then calculates the position and transmits it to MQTT. The obtained position is retrieved and recorded into the AGV through MQTT. For CCTV-based positioning, TP-Link Tapo C200 cameras are used, positioned at four locations. These cameras provide Full HD 1080p resolution and connect via the Real-Time Streaming Protocol (RTSP) to a computer, where the position is calculated. The computed position is then transmitted to MQTT and recorded into the AGV through MQTT. In the static experiment, 4 points are set: (1,1), (3,1), (1,7), and (3,7) by analysing UWB from the recorded distance values to select the measurement method, which has 2 types: RSSI and Tof. When the appropriate measurement method is obtained, the appropriate calculation method is selected, divided into 2 types: trilateration and triangular, to select the appropriate method and use the method used in the experiment together with CCTV to find the error value that occurs. The dynamic experiment focuses on testing AGV positioning while it moves in a straight line under predefined conditions. Position data is collected from both UWB and CCTV. An encoder attached to the motor is used, which counts the pulse width modulation (PWM) signals from the wheel encoders on both front wheels to calculate the position and record it directly into the AGV. Similarly, an IMU (WitMotion WT901C) is connected to the AGV and works with the encoder to compute the position, which is then recorded directly into the AGV. The UWB, encoder, and IMU sensors record data approximately every 0.1 seconds, while the CCTV records the most recently obtained values. From the position values read from each type of sensor, the weight Parallel Fusion method is used by using the weight value from the average of equal weights, from the weight value of the GRG method of each route, and the weight value of the GRG method of both routes combined. The results can be displayed according to the topic.

4.1 static experiments Results

Static experiment using 4 positions with the car facing in 4 directions. The experiment was repeated 3 times, and the experimental results can be presented as follows.

4.1.1 Comparing the ToF signal value with the RSSI value using 2 calculation methods: trilateration distance measurement and triangular distance measurement. It was found that the highest error value was at the x-axis RSSI value with a fault value of 9.2825 m (The trilateration is computed using anchor 4,1,2 at position (1,1) and angle 0 degree in the 2 experiment) meters and the y-axis error value was 7.6216 m (The triangular is computed using anchor 1,2 at position (3,1) and angle 90 degree in the 3 experiment). It was found that the RSSI value was higher than the ToF reading from the x-axis with a maximum error of 1.4828 m (The triangular is computed using anchor 3,4 at position (1,7) and angle 270 degree in the 2 and 3 experiment), and the y-axis had the highest error value of 1.8054 m (The triangular is computed using anchor 4,1 at position (3,7) and angle 180 degree in the 2 and 3 experiment). It was found that the ToF reading method should be selected based on the results of the experiment as shown in Table 1.

Table 1: Summary of error results comparing ToF and RSSI with two calculation methods.

Comparison	**Case/Method**	**Key Finding (Error Value)**	**Conclusion**
RSSI Maximum Error	Trilateration (Anchor 4,1,2; pos (1,1); angle 0°; Exp 2)	9.2825 m (x-axis)	RSSI has very high error.
RSSI Maximum Error	Triangular (Anchor 1,2; pos (3,1); angle 90°; Exp 3)	7.6216 m (y-axis)	RSSI error is unstable in y-axis.
ToF vs. RSSI (Difference)	Triangular (Anchor 3,4; pos (1,7); angle 270°; Exp 2-3)	ToF lower by 1.4828 m (x-axis)	ToF more reliable than RSSI.
ToF vs. RSSI (Difference)	Triangular (Anchor 4,1; pos (3,7); angle 180°; Exp 2-3)	ToF lower by 1.8054 m (y-axis)	ToF more reliable than RSSI.

4.1.2 In comparison of the use of the 3P method (trilateration) and the 2P method (triangular), the maximum error of the x-axis using the triangular method is 1.4824 m (The triangular is computed using anchor 3,4 at position (1,7) and angle 270 degree in the 2 and 3 experiment), the maximum error value of the y-axis when using the triangular method is -1.8054 m (The triangular is computed using anchor 4,1 at position (3,7) and angle 180 degree in the 2 and 3 experiment), the maximum error value of the x-axis when using the trilateration method is 1.4464 m (The

trilateration is computed using anchor 1,2,3 at position (1,7) and angle 90 degree in the 2 and 3 experiment), and the maximum error value of the y-axis when using the triangular method is 1.0464 m (The trilateration is computed using anchor 4,1,2 at position (1,1) and angle 180 degree in the 2 and 3 experiment) as shown in Table 2.

4.1.3 When comparing the positions of the anchors used in the calculations. When at position X=1 Y=7, which is close to position 2,3,4 and has the least error value. Position X=3 Y=1, which is close to position 1,2,3, found that the calculation from anchor points 4,1,2 had the lowest error value, but position 1,2,3 had a lower error value as shown in Table 3. It was found that 2 out of 4, the nearest calculation position has the least error value. Therefore, the nearest Anchor placement position was selected for calculation.

Table 2: The table shows the static error test.

Type	**Reading**	**Method**	**x (m)**	**y (m)**
UWB	RSSI	Trilateration	9.2825	—
	RSSI	Triangular	—	7.6216
	ToF	—	1.4828	1.8054
	ToF	Trilateration	1.4464	1.0464
CCTV	—	—	0.087	0.214

Table 3: The error results using ToF trilateration calculation.

Position		**RMSE (Anchor Combination)**			
x	**y**	**1,2,3**	**2,3,4**	**3,4,1**	**4,1,2**
1	1	0.75	0.92	1.23	1.12
3	7	0.77	0.68	0.55	0.58
1	7	0.96	0.74	0.33	0.56
3	1	0.51	0.76	0.96	0.77

4.1.4 The comparison between UWB and CCTV can be shown in Figure 11. when comparing the real position with the CCTV position obtained using the method of vision-based localization algorithm, and the UWB position obtained from CCTV is more accurate. Less dispersed. The positioning accuracy analysis CCTV shows that at position (1,1) with an orientation of 270 degrees, the maximum X error was 0.087 m, with an RMSE of 0.057061 m. At position (1,7) with an orientation of 180 degrees, the maximum Y error was 0.214 m, with an RMSE of 0.097567 m. The overall total RMSE for the system was 0.113028 m.

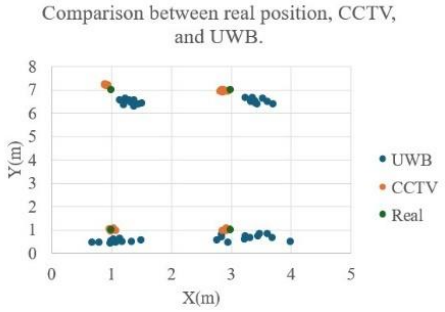

Figure 11. Comparison between real position, CCTV, and UWB.

The results of the error values that occurred in the static experiment can be summarized as shown in Table 2.

4.2 Dynamic experiment Results

Dynamic experiment by testing 2 speeds at average speeds of 0.4 and 0.27 m/s, which is given the starting point at x = 1, y = 0, moving in a straight line with the wheel radius of 0.052 m, and the distance between the wheels of 0.379 m, and the experimental results can be presented as follows.

4.2.1 Once the starting position is set, collect data that reads the Pulse Width Modulation (PWM) from the direction encoder from the speed difference of the two wheels (Encoder). Compare the direction obtained from the IMU (Encoder + heading (IMU)) using the moving speed from the average of the two wheels. The first path of the movement moved from the position x = 1, y = 0 to x = 0.48, y = 7.68 m with the locomotive starting at an angle of 93.87°, the second path moved from the position x = 1, y = 0 to x = 0.67, y = 8 m with the starting head at an angle of 92.4°. It can be done as shown in Figure 12(a), 12(b).

When implementing each type of sensor, it can be displayed as in Figure 13(a)., 13(b). Selected to calculate the position from encoder + heading (IMU) at a speed of 0.4 m/s with a root mean square error (RMSE) of 0.0035 m (x-axis) 0.0731 m(y-axis) and a total RMSE value of 0.0732 m with a maximum error of 0.0101 m(x-axis at(0.48,7.68)) 0.048 m(y-axis at(0.496421,7.437474)), speed 0.27 m/s with a RMSE of 0.0021 m (x-axis) 0.0678 m(y-axis) and a total RMSE value of 0.0678 m with a maximum error of 0.0034 m (x-axis at (0.7169,6.861)) 0.1086 m(y-axis at (0.7046,7.1593)), calculate the position from UWB at a speed of 0.4 m/s with a RMSE of 0.3317 m (x-axis) 1.1858 m (y-axis) and a total RMSE value of 1.2313 m with a maximum error of 0.6562 m(x-axis at(0.956211,0.646737)) 2.2 m(y-axis at(0.48,7.68)), speed 0.27 m/s with a RMSE of 0.2591 m (x-axis) 0.5156 m(y-axis) and a total RMSE value of 0.5770 m with a maximum error of 0.4053 m (x-axis at (0.704678,7.159322)) 0.82 m (y-axis at (0.67,7.8), calculate the position from CCTV at a speed

of 0.4 m/s with a RMSE of 0.1769 m (x-axis) 0.3951 m (y-axis) and a total RMSE value of 0.4329 m with a maximum error of 0.3449 m(x-axis at(0.770105,3.395368) 0.7537 m(y-axis at(0.660632,5.012211)), speed 0.27 m/s with a RMSE of 0.2414 m (x-axis) 0.2628 m (y-axis) and a total RMSE value of 0.3568 m with a maximum error of 0.3725 m(x-axis at (0.932881,1.627119)) 0.4795 m(y-axis at (0.827729,4.176271)). It can be seen that the movement in a straight line is calculated from encoder + heading (IMU). The lowest error rate is followed by CCTV and UWB respectively. When considering the speed, it can be seen that the higher the speed of UWB, the higher the error rate. The integration of the encoder and IMU produced the most accurate localization due to the synergy between dead reckoning and drift correction. While encoders provide incremental movement data, the IMU stabilizes heading estimations, minimizing angular deviation over time. At higher speeds, UWB readings suffered from increased positioning errors. This is primarily attributed to multipath propagation effects and signal delays that occur during rapid movement, affecting both RSSI and ToF estimations. CCTV localization demonstrated high stability under consistent lighting conditions. As the vision algorithm depends on contrast, environments with fixed illumination enhance detection performance and reduce positioning fluctuations.

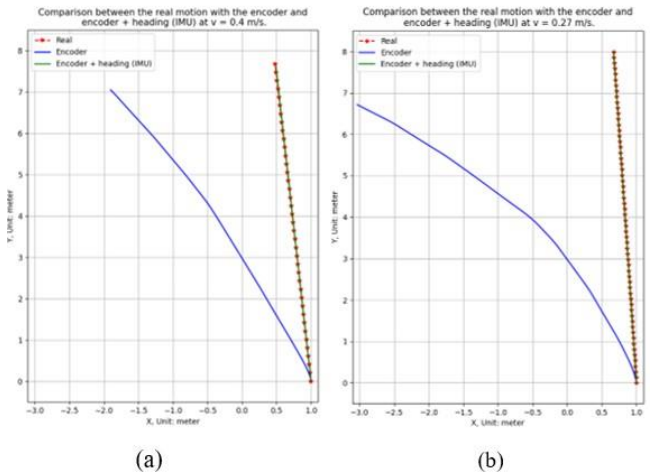

Figure 12. Comparison the real motion with the encoder and encoder + heading (IMU) (a) at v = 0.4 m/s. (b) at v = 0.27 m/s.

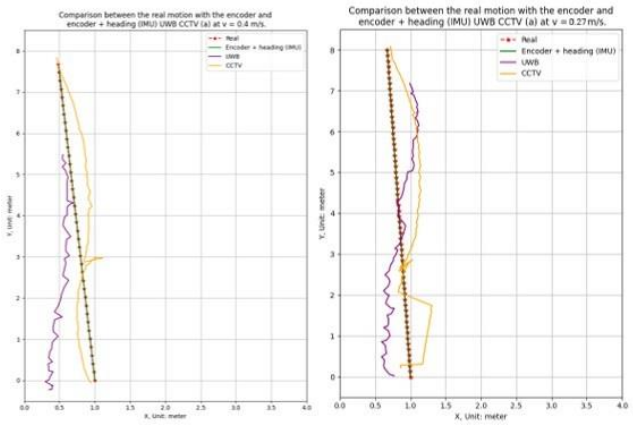

(a) (b)

Figure 13. Comparison real motion with encoder and encoder + heading (IMU) UWB CCTV at (a) v = 0.4 m/s. (b) v = 0.27 m/s.

4.2.2 Using a Fusion sensor in parallel, as shown in Figure 14(a)., 14(b). At a speed of 0.4 m/s using the average weight value, the RMSE of 0.1470 m(x-axis) 0.5241 m(y-axis), and a total RMSE value of 0.5444 m with a maximum error of 0.3248 m(x-axis) 1.124 m(y-axis). At a speed of 0.27 m/s using the average weight value, the RMSE of 0.1681 m(x-axis) 0.2732 m(y-axis), and a total RMSE value of 0.3208 m with a maximum error of 0.2317 m(x-axis) 0.3840 m(y-axis).

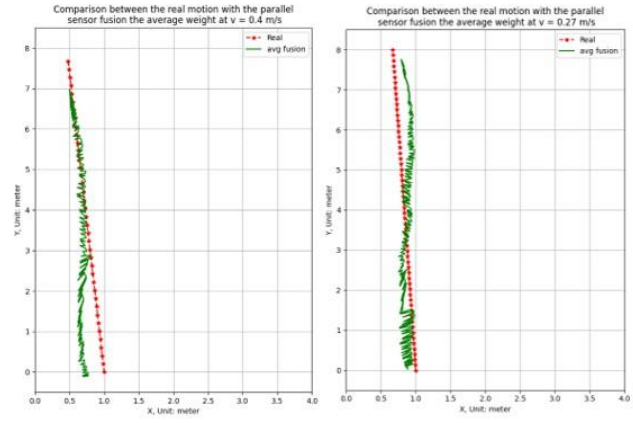

(a) (b)

Figure 14. Comparison real motion with parallel sensor fusion using average weight at (a) v = 0.4 m/s. (b) v = 0.27 m/s.

4.2.3 Use Weighted Parallel Fusion from the optimization in the Excel program for each movement path. When testing the optimal parameter of the sensor weight multiplier, there are two conditions. The first condition is when the sensor values are transmitted completely, allowing them to be used as described in Equation 9.

$$(x,y) = \frac{a \cdot (Encoder + IMU\ heading)(x,y)}{a + b + c} + \frac{b \cdot UWB(x,y) + c \cdot CCTV(x,y)}{a + b + c} \quad (9)$$

The second condition is when the sensor values are not completely transmitted, and there are no values from the CCTV sensor. In this case, use Equation 10. instead.

$$(x,y) = \frac{d \cdot (Encoder + IMU\ heading)(x,y)}{d + e} \qquad (10) \qquad + \frac{e \cdot UWB(x,y)}{d + e}$$

The optimal parameter values can be found from the Excel program by selecting the GRG Nonlinear method, which is shown in Table 4, showing weight values used for optimal at a speed of 0.4 m/s and having the RMSE of 0.009 m(x-axis) 0.0616 m(y-axis), and a total RMSE value of 0.0623 m with a maximum error of 0.0211 m(x-axis) 0.1164 m(y-axis) shown as Figure 15(a). the optimal parameter values shown Table 5, weight values used for optimal at a speed of 0.27 m/s and having the RMSE of 0.1681 m(x-axis) 0.2732 m(y-axis), and a total RMSE value of 0.3208 m with a maximum error of 0.2317 m(x-axis) 0.3840 m(y-axis) shown as Figure 15(b).

Table 4: The weight values used for optimal at a speed of 0.4 m/s.

a	**b**	**c**	**d**	**e**
0.0617	0.00027	0.0038	1.7673	0.0580

4.2.4 Use Weighted Parallel Fusion from the optimization in the Excel program obtained by combining all paths. From Figure 16(a)., 16(b). and Table 6, weight values used for optimal at all speeds have an RMSE value of 0.4 m/s which is 0.0154 m(x-axis) 0.0647 m(y-axis), and a total RMSE 0.0591 m(y-axis), and a total RMSE value of 0.0634 m with a maximum error of 0.035 m(x-axis) 0.0894

m(y-axis) shown in the Table 7 is the results of the dynamic experiment can be Summarized. value of 0.0665 m with a maximum error of 0.027 m(x-axis) 0.153 m(y-axis), and an SSE value of 0.27 m/s which is 0.0228 m(x-axis)

Table 5: The weight values used for optimal at a speed of 0.27 m/s.

a	**b**	**c**	**d**	**e**
2.4332	0.1679	0.1057	2.1349	0.2070

Table 6: The weight values used for all optimal at all speed.

a	**b**	**c**	**d**	**e**
0.1176	0.0037	0.0106	1.9884	0.1019

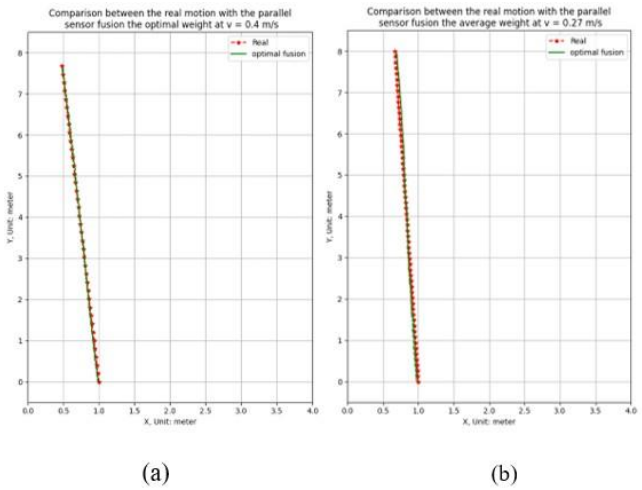

(a) (b)

Figure 15. Comparison real motion with parallel sensor fusion using the optimal weight at (a) v = 0.4 m/s. (b) v = 0.27 m/s.

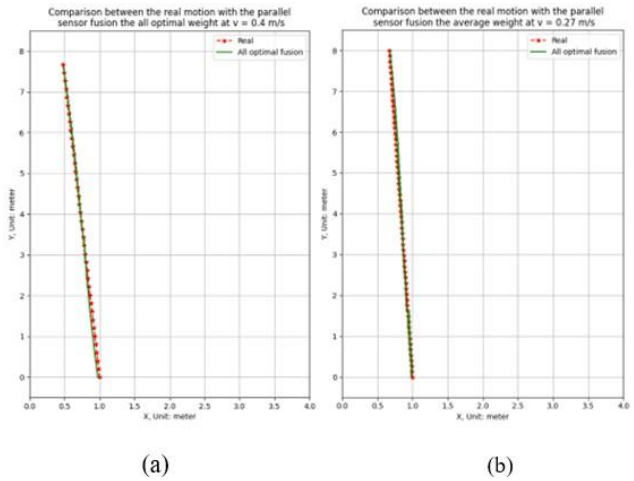

(a) (b)

Figure 16. Comparison real motion with parallel sensor fusion using the optimal weight at (a) v = 0.4 m/s. (b) v = 0.27 m/s.

Table 7: The dynamic error test results.

Type	**Speed (m/s)**	**Max Error (m)**	**RMSE**	**RMSE(x, y)**	**x**	**y**
encoder	0.4	0.0805	0.1226	0.0526	0.0707	0.0881
Encoder + IMU		0.0101	0.0480	0.0035	0.0731	0.0732
UWB		0.6562	2.2000	0.3317	1.1858	1.2313
CCTV		0.3449	0.7537	0.1769	0.3951	0.4329
AVG Fusion		0.3248	1.1240	0.1470	0.5241	0.5444
opt Fusion		0.0211	0.1164	0.0090	0.0616	0.0623
All opt Fusion		0.0270	0.1530	0.0154	0.0647	0.0665
encoder	0.27	0.0979	0.1070	0.0637	0.0642	0.0904
Encoder + IMU		0.0034	0.1086	0.0021	0.0678	0.0678
UWB		0.4053	0.8200	0.2591	0.5156	0.5770
CCTV		0.3725	0.4794	0.2414	0.2628	0.3568
AVG Fusion		0.2317	0.3840	0.1681	0.2732	0.3208
opt Fusion		0.0328	0.0690	0.0199	0.0360	0.0411
All opt Fusion		0.0350	0.0894	0.0228	0.0591	0.0634

5. Conclusion

This research developed and validated a low-cost, multi-sensor fusion system for indoor AGV localization, presenting a viable alternative to expensive LiDAR-based solutions. By integrating data from encoders, IMUs, UWB, and CCTV through a parallel fusion architecture optimized with a Generalized Reduced Gradient (GRG) algorithm, we demonstrated a significant enhancement in positioning accuracy. Our findings reveal several key insights. In static tests, the Trilateration method proved more robust than the Triangular method for UWB

positioning, reducing maximum errors to 1.4464 m (x-axis) and 1.0464 m (y-axis). For dynamic localization, the synergy between the encoder and IMU was paramount, yielding the lowest RMSE of 0.0732 m at 0.4 m/s and 0.0678 m at 0.27 m/s. This highlights the effectiveness of combining dead-reckoning data with drift correction from the IMU. Conversely, UWB performance degraded at higher velocities, likely due to multipath propagation and signal delays, while CCTV provided stable, albeit less accurate, localization The most significant contribution of this work is the application of the GRG-optimized weighted fusion, which reduced the final RMSE to as low as 0.0623 m and 0.0411 m at 0.4 m/s and 0.27 m/s, respectively. This demonstrates that a carefully weighted combination of low-cost sensors can achieve the high level of accuracy required for many industrial applications, directly addressing the cost barrier of widespread AGV adoption. While these results are promising, we acknowledge certain limitations. The experiments were conducted in a controlled environment with predefined, straight-line paths. In addition, the GRG weight adjustment is performed offline. The current system uses constant weight. Furthermore, its practical application in industrial environments presents significant challenges, such as noise from machinery and uncontrolled environments. Future research should explore more complex paths and dynamic environments. Future work will focus on four primary areas. First, we plan to implement a real-time adaptive weighting mechanism, possibly using machine-learning algorithms like neural networks, to dynamically adjust sensor weights without manual optimization. Second, integrating Kalman filtering could further mitigate sensor noise and improve state estimation. Third, integrating the system with an IoT platform allows for real-time tracking of multiple AGVs, route planning, and data analysis for process optimization within the framework of a smart factory. Finally, deploying and testing the system in a live warehouse environment will be crucial to validate its practical applicability and robustness.

Acknowledgments: "This research is gratefully acknowledged for the support from Suranaree University of Technology and Department of Mechatronics and Robotics Engineering, School of Engineering and Innovation, Rajamangala University of Technology Tawan-ok. Thailand."

Funding: "This work was supported by Suranaree University of Technology."

Conflicts of Interest: "The authors declare no conflict of interest."

References

[1] I. Kubasakova, J. Kubanova, D. Benco, and D. Kadlecová, "Implementation of Automated Guided Vehicles for the Automation of Selected Processes and Elimination of Collisions between Handling Equipment and Humans in the Warehouse," *Sensors*, vol. 24, no. 3, 2024.

[2] A. Thakur and P. Rajalakshmi, "LiDAR-Based Optimized Normal Distribution Transform Localization on 3-D Map for Autonomous Navigation," *IEEE Open Journal of Instrumentation and Measurement*, vol. 3, pp. 1-11, 2024.

[3] K. W. Park and S. Y. Park, "Visual LIDAR Odometry Using Tree Trunk Detection and LIDAR Localization," *The International Archives of the Photogrammetry, Remote Sensing and Spatial Information Sciences*, vol. XLVIII-1/W2-2023, pp. 627-632, 2023.

[4] N. Maitlo, N. Noonari, K. Arshid, N. Ahmed, and S. Duraisamy, "AINS: Affordable Indoor Navigation Solution via Line Color Identification Using Mono-Camera for Autonomous Vehicles," in *2024 IEEE 9th International Conference for Convergence in Technology (I2CT)*, 2024, pp. 1-7.

[5] S. Jeong, M. Ko, and J. Kim, "LiDAR Localization by Removing Moveable Objects," *Electronics*, vol. 12, no. 22, 2023.

[6] S. Odngam, P. Intacharoen, N. Tanman, and C. Sumpavakup, "The Design of Distance-Warning and Brake Pressure Control Systems Incorporating LiDAR Technology for Use in Autonomous Vehicles," *World Electric Vehicle Journal*, vol. 15, no. 12, 2024.

[7] F. Sauerbeck, D. Kulmer, M. Pielmeier, M. Leitenstern, C. Weiß, and J. Betz, "Multi-LiDAR Localization and Mapping Pipeline for Urban Autonomous Driving," in *2023 IEEE SENSORS*, 2023, pp. 1-4.

[8] M. Kascha, K. Xin, X. Zou, A. Sturm, R. Henze, L. Heister, and S. Oezberk, "Monocular Camera Localization for Automated Driving," in *2023 29th International Conference on Mechatronics and Machine Vision in Practice (M2VIP)*, 2023, pp. 1-6.

[9] T. Kim, S. Lim, G. Shin, G. Sim, and D. Yun, "An Open-Source Low-Cost Mobile Robot System With an RGB-D Camera and Efficient Real-Time Navigation Algorithm," *IEEE Access*, vol. 10, pp. 127871-127881, 2022.

[10] L. Triyono, R. Gernowo, and P. Prayitno, "Optimizing indoor navigation systems through ensemble deep learning techniques for ArUco marker detection," *International Journal of Intelligent Engineering & Systems*, vol. 17, no. 6, 2024.

[11] X. Liu, G. Wang, and K. Chen, "High-precision vision localization system for autonomous guided vehicles in dusty industrial environments," *NAVIGATION: Journal of the Institute of Navigation*, vol. 69, no. 1, 2022.

[12] S. Y. Alaba, "GPS-IMU Sensor Fusion for Reliable Autonomous Vehicle Position Estimation," *ArXiv*, vol. abs/2405.08119, 2024.
[13] A. Charroud, K. El Moutaouakil, V. Palade, and A. Yahyaouy, "Enhanced autoencoder-based LiDAR localization in self-driving vehicles," *Applied Soft Computing*, vol. 152, p. 111225, 2024.
[14] V. Brunacci, A. Dionigi, A. De Angelis, and G. Costante, "Infrastructure-less UWB-based Active Relative Localization," in 2024 IEEE/RSJ International Conference on Intelligent Robots and Systems (IROS), 2024, pp. 14079-14086.
[15] K. Wongvichayakul, C. Mitsantisuk, and K. Prompol, "Development of high-precision ultra-wideband (UWB) path following using Kalman filter for automatic guide vehicles," in *Proceedings of IECON 2023 - 49th Annual Conference of the IEEE Industrial Electronics Society*, 2023, pp. 1-6.
[16] M. Kim, Y. Kwon, S. Lee, and S.-e. Yoon, "CCTV-informed human-aware robot navigation in crowded indoor environments," *IEEE Robotics and Automation Letters*, vol. 9, no. 6, pp. 5767-5774, 2024.
[17] C. Lundquist, *Sensor Fusion for Automotive Applications*, Ph.D. dissertation, Linköping University, Linköping, Sweden, 2011.
[18] Y. Chandola, J. Virmani, H. S. Bhadauria, and P. Kumar, "Chapter 4 - End-to-end pre-trained CNN-based computer-aided classification system design for chest radiographs," in *Deep Learning for Chest Radiographs, Primers in Biomedical Imaging Devices and Systems*, Academic Press, 2021, pp. 117-140.
[19] R. A. Pashchapur, Y. Chen, and D. Ignatyev, "Low–cost multi-object positioning system with optical sensor fusion," in *AIAA SCITECH 2023 Forum*, AIAA SciTech Forum, American Institute of Aeronautics and Astronautics, Jan. 2023.
[20] W. Zhu and S. Guo, "Indoor Positioning of AGVs Based on Multi-Sensor Data Fusion Such as LiDAR," *International Journal of Sensors and Sensor Networks*, vol. 12, no. 1, pp. 13-22, 2024.
[21] S. Bouzoualegh, E.-H. Guechi, and R. Kelaiaia, "Model Predictive Control of a Differential-Drive Mobile Robot," *Acta Universitatis Sapientiae Electrical and Mechanical Engineering*, vol. 10, pp. 20-41, Dec. 2018.
[22] R. Dhaouadi and A. A. Hatab, "Dynamic Modelling of Differential-Drive Mobile Robots using Lagrange and Newton-Euler Methodologies: A Unified Framework," in *Proc. IEEE Int. Conf. on Robotics and Automation*, vol. 02, 2013.
[23] E. Alcalá, L. Sellart, V. Puig, J. Quevedo, J. Saludes, D. Vázquez, and A. López, "Comparison of two non-linear model-based control strategies for autonomous vehicles," in *Proceedings of the 24th Mediterranean Conference on Control and Automation (MED)*, 2016, pp. 846-851.
[24] F. Che, Q. Z. Ahmed, P. I. Lazaridis, P. Sureephong, and T. Alade, "Indoor Positioning System (IPS) using Ultra-Wide Bandwidth (UWB)-for Industrial Internet of Things (IIoT)," *Sensors*, vol. 23, no. 12, article no. 5710, 2023.
[25] Z. Chen, X. Li, L. Wang, Y. Shi, Z. Sun, and W. Sun, "An Object Detection and Localization Method Based on Improved YOLOv5 for the Teleoperated Robot," *Applied Sciences*, vol. 12, no. 22, pp. 11441, 2022.
[26] L. S. Lasdon, R. L. Fox, and M. W. Ratner, "Nonlinear optimization using the generalized reduced gradient method," *Recherche Opérationnelle*, vol. 8, no. 3, pp. 73-103, 1974.
[27] L. S. Lasdon, A. D. Waren, A. Jain, and M. Ratner, "Design and testing of a generalized reduced gradient code for nonlinear programming," *ACM Transactions on Mathematical Software*, vol. 4, no. 1, pp. 34-50, Mar. 1978.
[28] J. S. Arora, "Chapter 13 - More on Numerical Methods for Constrained Optimum Design," in *Introduction to Optimum Design (Third Edition)*, Academic Press, 2012, pp. 533-573.
[29] D. B. Nugroho, L. P. Panjaitan, D. Kurniawati, Z. Kholil, B. Susanto, and L. R. Sasongko, "GRG non-linear and ARWM method for estimating the GARCH-M, GJR, and log-GARCH models," *Jurnal Teoridan Aplikasi Matematika*, vol. 6, no. 2, pp. 448-460, 2022.
[30] S. J. Terregrossa and U. S¸ener, "Employing a generalized reduced gradient algorithm method to form combinations of steel price forecasts generated separately by ARIMA-TF and ANN models," *Cogent Economics & Finance*, vol. 11, no. 1, 2023.